A purely kinetic description of the evaporation of water droplets

Frances A. Houle[a]*, Rachael E. H. Miles[b], Connor J. Pollak[c] and Jonathan P. Reid[b]

[a]Joint Center for Artificial Photosynthesis and Chemical Sciences Division, Lawrence Berkeley National Laboratory, Berkeley, CA 94720, USA
[b] School of Chemistry, University of Bristol, Bristol, BS8 1TS, UK
[c] Department of Chemical and Biomolecular Engineering, University of California, Berkeley, CA 94720, USA

ABSTRACT

The process of water evaporation, although deeply studied, does not enjoy a kinetic description that captures known physics and can be integrated with other detailed processes such as drying of catalytic membranes embedded in vapor-fed devices and chemical reactions in aerosol whose volumes are changing dynamically. In this work, we present a simple, 3-step kinetic model for water evaporation that is based in theory, and validated using well-established thermodynamic models of droplet size as a function of time, temperature and relative humidity as well as data from time-resolved measurements of evaporating droplet size. The kinetic mechanism for evaporation is a combination of two limiting processes occurring in the highly dynamic liquid-vapor interfacial region: direct first order desorption of a single water molecule, and desorption resulting from a local fluctuation, described using third order kinetics. The model reproduces data over a range of relative humidities and temperatures only if the interface that separates bulk water from gas phase water has a finite width, consistent with previous experimental and theoretical studies. The influence of droplet cooling during rapid evaporation on the kinetics is discussed; discrepancies between the various models point to the need for additional experimental data to identify their origin.

INTRODUCTION

The physics of water evaporation enjoys a vast literature, and examples of studies range from kinetic[1, 2] and statistical mechanical[3-6] to continuum thermodynamics[7, 8] treatments on the computational side, to direct measurements of molecular characteristics of the water interface[9-11] and evaporation of pools and droplets in contact with vacuum, water vapor, and humidified inert gas.[12-20] A quantitative understanding of the rate of water evaporation is essential in situations ranging from cloud chemistry[21] to membrane-electrode assemblies used in vapor-fed electrochemical CO_2 conversion systems,[22] in order to predict how the reactive environment changes with time and relative humidity (RH). Although the ubiquitous evaporation process is still not completely understood, a physical picture has emerged. Liquid water is volatile near ambient temperature and, excepting when evaporating into vacuum, the liquid is always in contact with its vapor, whose gas phase concentration at a temperature defines a local RH. The two basic chemical steps involved in evaporation and condensation are therefore that a water molecule can break its hydrogen bonds and detach from the liquid, and a water molecule in the vapor phase can impinge on the liquid, and will stick to it. Accordingly, at steady state there is a balance between evaporation and condensation. This steady state is often equated to microscopic reversibility of adsorption and desorption, enabling treatments of net evaporation to be formulated and estimates to be made of the condensation and evaporation coefficients.[2, 5, 12, 21, 23-28] Whether or not microscopic reversibility is correct is under debate, and a deeper understanding of the specific dynamics of desorption and adsorption will help clarify this question.

The coupling of condensation and evaporation is embedded in models based on gas kinetics such as the Hertz-Knudsen model,[3, 6] which consider mass fluxes to and from the water-vapor

interface, and comprehensive statistical rate theory and thermodynamics models such as the Kulmala model [6, 7, 18] and the Liu model[18, 29] that take into account the coupling between mass and energy fluxes in the gas-liquid environment. An important question associated with this coupling concerns the temperature at the water-vapor boundary. Experimental and theoretical studies have reported both the presence[3, 4, 6, 13, 17, 27] and the absence[5, 14, 30, 31] of a temperature lower than ambient at the liquid-vapor interface, and considered how thermal equilibrium between the two phases depends on the evaporation rate.[26] This is a complex question: studies of planar water layers showing minimal interfacial cooling even during rapid evaporation[30, 31] reflect rather different conditions than those in small droplets, which cool due to their limited heat capacity.[27]

Theories describing macroscopic phenomena in terms of fluxes are valuable to model overall behavior of a system, but do not include the molecular structure and dynamics of the gas-liquid interface for water, that is, the local environment or molecular motions by which condensation and evaporation take place. The interfacial region directly involved in evaporation has been the subject of extensive study for both droplets (which have a curved surface) and water pools (which have a flat surface).[5, 9, 26, 32-40] That the interfacial width is finite was recognized in studies of the nature of surface tension and how it scales with the size of a droplet. Studies of Lennard-Jones fluids have shown that the transition between a completely liquid state and a completely vapor state takes place over a finite distance due to the nature of the interaction potentials.[36, 38, 40] In the specific case of water, where chemical interactions are present in addition to dispersion interactions, the interface has reduced density due to the disruption of the hydrogen-bonding structure, and to the presence of molecular scale capillary waves.[9, 33-35, 41] The thickness of the

water interfacial region has been studied both theoretically and experimentally, and increases approximately exponentially with temperature.[32, 37, 42, 43] The interface belonging to an evaporating droplet has approximately constant thickness at a given temperature until it reaches < 50 nm, when it increases as the surface tension of the droplet decreases.[39]

The studies of the water-vapor system provide important insights, but because of their mathematical forms do not enable construction of chemical mechanisms involving elementary steps that can be used to couple the kinetics of evaporation with chemical reactions and transport through heterogeneous environments such as polymers, which occur at the same time on native timescales (many seconds). Having the ability to correctly model aqueous chemistry in a solution whose volume is continuously changing - leading to continuously changing reagent and product concentrations - is essential to understand many systems in the laboratory and in nature, including those where reactivity appears to be influenced by confinement such as droplets.[44, 45] Progress toward construction of such elementary steps has been reported in two recent studies. A comparison has been made between molecular dynamics simulations of evaporation and a kinetic description that took into account the complex structure of water at the gas-liquid interface for flat surfaces and droplets of about 2 and 4 nm radius.[2] It was concluded in that work that a simple kinetic description of evaporation and condensation in terms of water molecules detaching and attaching at the gas-liquid interface was sufficiently detailed to capture the essential physics. A subsequent molecular dynamics study[46] provided a rather different picture, however. That work showed that water evaporation is a third order process in which motion of 3 waters coupled by 2 pairwise interactions is required for hydrogen bond formation and breakage, and detachment of a water from the liquid. The physical picture that liquid structure fluctuations

involving hydrogen bonds are required for desorption is consistent with calculations that showed that desorption occurs at interfaces having negative curvature due to collective water fluctuations.[5]

Which of these kinetic descriptions applies? The third order process is not just a completely concerted motion of 3 molecules, rather, it involves interactions occurring over a range of times.[46] This suggests that both may be correct, with one limiting case being a simple hydrogen-bond breaking step as had been proposed previously,[2] and the other being a pure third order step. These two cases are illustrated in Figure 1.

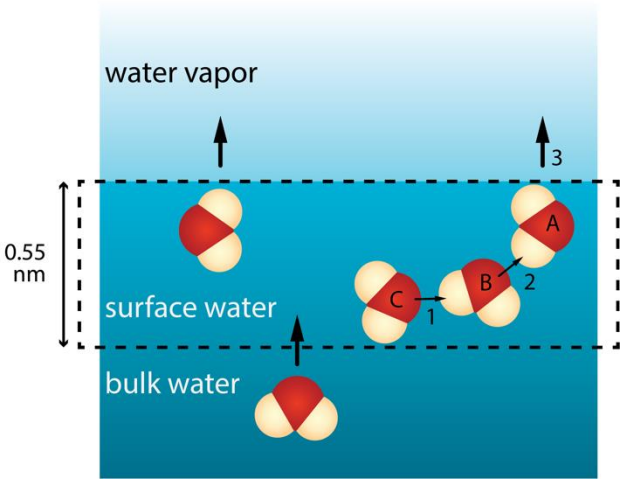

Figure 1. The water evaporation mechanism consists of 2 processes: simple first order desorption, and a third order desorption resulting from the steps of molecules C and B forming a hydrogen bond, and B colliding with A shortly after to transfer sufficient momentum for it to leave the liquid state. As surface water evaporates, bulk water diffuses to replace it.

In the computational and experimental study reported here, we evaluate this simple chemical kinetic scheme for water evaporation, which embodies the assumption that these 2 limiting cases

can represent what is in actuality a continuum of pairwise interactions leading to water desorption. The model also builds the influences on the evaporation process of a diffuse water surface region and an interface that spans pure vapor and pure liquid phases. Simulations of droplet evaporation rather than large pool evaporation are an ideal test of the validity of this kinetic scheme: the kinetic mechanism alone must correctly predict that the droplet's radius r decreases as $1/r^2$ vs time.[19] The kinetics simulation results are compared to droplet evaporation measurements and the results of thermodynamic model calculations over a relative humidity range of 55-98% in a background gas at atmospheric pressure, a temperature range of 278-318K and a droplet diameter range of 10-50 μm. Under these conditions, the droplet diameter is much larger than the mean free path of the gases present (about 70nm) until the final few ms, and the kinetic simulations correspond almost entirely to a diffusive (or continuum) gas-droplet interaction regime. The data presented in the Results section show that agreement with measurements and the Kulmala model is good, however there are systematic deviations from the Liu model. The calculations also provide predictions for droplet radius as a function of time down to complete evaporation where data are currently unavailable, and insights to the kinetic importance of first and third order desorption as a function of time and droplet size.

METHODS

Continuum modeling

Two different continuum models were used in this work to simulate water evaporation profiles for comparison to the kinetic scheme over a wide range of conditions. Both models, the Kulmala model and the Liu model, have been benchmarked in previous studies and have been shown to accurately model the evaporation of water droplets under a range of different RH and

temperature conditions.[12, 17, 18, 21, 47] Differences in the way that the two models treat droplet evaporative cooling mean that the Kulmala model can be used under conditions where evaporative cooling is low (< 3K), while the Liu model is able to successfully account for greater degrees of surface cooling.

Kinetic model construction

The simulations performed in this work use a stochastic method to solve the master equation for the system, embodied in the open-access package *Kinetiscope*.[48] The core algorithm[49, 50] is a type of kinetic Monte Carlo calculation that predicts concentrations *vs* an absolute time base for direct comparison to experimental observations. When applied to evaporation of a water droplet into a humid gas environment, several factors must be included in the simulations besides the desorption events themselves: the opposing condensation and evaporation fluxes due to the finite vapor pressure of water in the surrounding gas, the existence of a density gradient at the liquid surface due to disruptions in the hydrogen bonded structure of water, the existence of a thicker interfacial region transitioning between pure liquid and pure vapor phases, and a continuously increasing surface/volume ratio as the droplet evaporates. Thermodynamic treatments also include heat flux, however this aspect of the physics is not included in this model and thermal equilibrium between the vapor and the liquid in the interfacial region is assumed. Discussion of the impact of this approximation is presented later in this paper. In this section, how each of these factors has been built into the model and the values for the variables used in the simulations are described.

The simulated droplet is represented as a single compartment using a technique introduced previously, which properly weights the surface/volume ratio as the droplet shrinks.[44] Briefly, as illustrated in Figure 2, the compartment is defined as a cuboid with a height 1/3 of the droplet radius *r* (*r* is typically 25 μm), with one end at the droplet surface, and the other in the bulk. The measured experimental starting radius is used in the simulations. The area of the ends is defined to be 1 μm^2. The surface end where desorption events can occur is defined to have a finite thickness of 0.55 nm based on electronic structure calculations.[35] This value is in the mid-range of estimates of 0.3 - 0.8 nm for an interfacial region in the literature,[5, 9, 33-35, 42] which includes capillary waves as well as an electron density gradient. The defined surface region is represented by an amount of surface waters within the compartment, defined to be located only at the surface. The remaining water is defined to be bulk waters. The total initial amount of water in the compartment is determined using the starting volume of the droplet and the density of water at 273.15K, 0.9983 g/cm^3.[51] Temperature-dependent densities are used, however they vary only slightly in this range. As water evaporates, the area of the initially defined surface region and its thickness remain constant. This constraint ensures that the height of the compartment corresponding to the liquid phase scales with droplet radius, and that the surface to volume ratio scales as 3/*r* from the initial radius of about 25 μm down to a radius of about 300 nm. The composition of the entire desorbed gas + droplet liquid system is explicitly tracked throughout the simulation, but only the volume of the liquid is continuously recalculated in order that instantaneous concentrations of bulk and surface water are correct. Gaseous desorbed water is assumed to not increase the surrounding system's RH due to the small amounts of water emanating from the droplet.

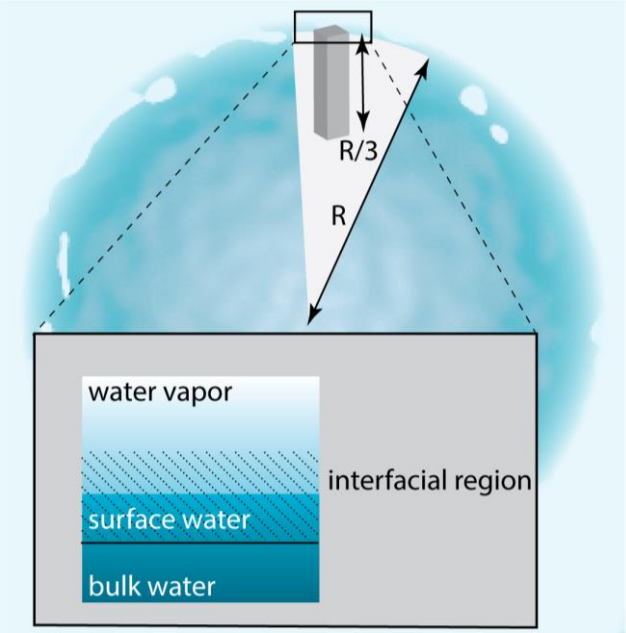

Figure 2. Illustration of simulation volume. The compartment is a rhomb with a top and bottom surface area of 1x1 μm, and a height of 1/3 the initial droplet radius, typically 8 μm. At the top of the compartment, the 0.55 nm thick surface water region is defined. The interfacial region separating bulk liquid water from water vapor has a temperature-dependent thickness that is used to convert the evaporating flux to a net evaporation rate coefficient.

Only water molecules located in the surface region can desorb. As noted above, the desorption mechanism is represented using two limiting cases that first and third order processes. A first order desorption step is written as

$$H_2O(surface\ liquid) \rightarrow H_2O(vapor) + site \quad (1)$$

and has a corresponding condensation step

$$H_2O(vapor) + site \rightarrow H_2O(surface\ liquid) \quad (2)$$

The condensation step is independent of droplet size and gas mean free path, and applies to the diffusive regime. The species *site* in (1) and (2) is provided to ensure that the amount of surface liquid waters remains constant at all times: it is formed when desorption occurs and consumed when a water molecule condenses. It is used throughout the mechanism as described further below. In stochastic kinetics calculations as implemented in *Kinetiscope*, the probabilities of evaporation and condensation are very close, and direct simulation of steps (1) and (2) is prohibitively inefficient. Therefore, we assume that the evaporation process is a net evaporation process, as written in (1), and is represented by the Hertz-Knudsen equation.[6] The net mass flux of water j^{LV} is

$$j^{LV} = \sqrt{\frac{m}{2\pi k_B}} \left(\sigma_e \frac{P_S(T^L)}{\sqrt{T_I^L}} - \sigma_c \frac{P^V}{\sqrt{T_I^V}} \right) \quad (3)$$

where m is the mass of H_2O, k_B is the Boltzmann constant, $P_S(T^L)$ is the saturation vapor pressure at the temperature of the liquid, and P^V is the partial pressure of the molecule in the vapor phase. The subscript I for T^L and T^V refers to the temperature of the liquid and vapor, respectively, at the liquid-vapor interface. These temperatures are assumed to be equal and constant during evaporation. σ_e and σ_c are the evaporation and condensation coefficients, and are equal if the processes are strictly reversible and at equilibrium. For the case of pure water, many studies have reported their values to be between 0.5 and 1.[21, 23-25, 27, 52] As a simplifying assumption, they are

taken to be 1 in this work. The saturation vapor pressure $P_S(T^L)$ is calculated using a published parameterization.[53]

The rate coefficient k_1 used in the simulation of step (1) as a net process is calculated from j^{LV}, which is converted to units of molecules/unit area-time for the simulations. The phase transition is from the liquid to the vapor phase, and this is not a process that takes place by simply crossing a plane: indeed evidence has been found for the presence of unbound water molecules in the near surface region of droplets,[11] which introduces ambiguity into the transition process. Accordingly, we assume that the transition between pure liquid and pure vapor occurs across a finite distance *d* that starts in the top surface layer of the defined compartment, which is a transition region spanning bulk water to the liquid-vapor interface (Figure 2). Therefore, desorption occurs from within a volume defined by the area of the top of the compartment and this distance. A schematic of the interfacial region as implemented in this work is shown in Figure 2. The rate coefficient in units of sec^{-1} is calculated as

$$k_1 = \frac{j^{LV}}{d\,[H_2O]} \qquad (4)$$

where the water concentration $[H_2O]$ is taken to be that of pure liquid water. This is an oversimplification: the density of water decreases significantly across this distance, and the value used can be refined when better experimental data become available.

Careful consideration was made for how to determine the magnitude of *d* since both measurements and calculations of it have been made on flat surfaces, but not on droplets. It is known that the thickness of the region associated with surface tension is greater for a curved surface than for a flat surface, and that according to the Kelvin effect the vapor pressure of water

above an evaporating droplet increases as the droplet becomes smaller.[38-40, 54] It is also known from theory[37, 43] and experiments that the thickness of the interfacial region spanning liquid water to vapor at ambient pressure is temperature-dependent.[42] Since the precise thickness is unknown for droplets, but must be at a minimum in the range of the theoretical and experimental values, in this work the thickness was treated as a fitting parameter for a series of measurements at a constant RH of 95% and temperatures from 318-273 K.

The second limiting case is written as a purely 3rd order process, which represents a closely associated two water-pair motion leading to desorption of one water molecule and creation of a vacant site at the surface.[46]

$$3\,H_2O(surface\ liquid) \rightarrow\ H_2O(vapor) +\ 2\,H_2O(surface\ liquid) + site \qquad (5)$$

To enable evaporation, a step is required that represents migration of water to the surface of the droplet. We assume that net transfer between the bulk water and the surface water occurs when a surface water has evaporated and a "site" is available for a bulk water. The transfer is written as

$$H_2O\ (bulk\ liquid) + site\ \rightarrow\ H_2O\ (surface\ liquid) \qquad (6)$$

The rate coefficient for this step is calculated from the self-diffusion coefficient of water at the temperature used in the simulations,[55] as $1/t$ sec^{-1}, where t is the time to traverse a distance of 1 nm and move from bulk water to anywhere in the surface region. This distance is an assumption, estimated from the geometry of the model (Figure 2).

A rate coefficient for step (5) is needed. In the molecular dynamics study of this limiting case, an overall net evaporative flux was estimated, but a rate coefficient was not reported. Therefore, we used simulations of the 3-step mechanism (steps (1), (5) and (6)) to determine a value for the rate coefficient for (5) for one temperature and relative humidity, assuming a thickness *d* of 1 nm which is the approximate difference between the surface thickness as determined by electron density and the total interfacial thickness for a flat water pool in equilibrium with its vapor at 300K.[37] Comparing to simulations using the Kulmala model, the best fit value for an RH of 98% and a temperature of 293.15 K is 3 x 10^{-36} $cm^6/molec^2$-sec. To obtain estimates for other RH and temperatures, we hypothesized that this coefficient scales in proportion to the scaling of the Hertz-Knudsen flux. This is motivated by the physical picture that desorption via the 2-water-

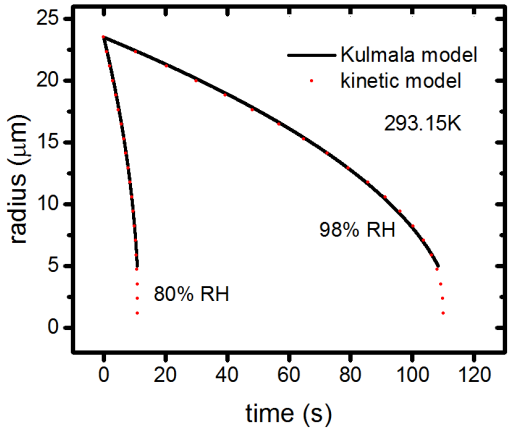

Figure 3: Comparison of kinetic model predictions with those of Kulmala model at a temperature of 293.15K. The 98% RH curve was obtained by treating the unknown rate coefficient of the 3rd order desorption step as a fitting parameter. The 80% RH curve was predicted by assuming that the 3rd order rate coefficient scales with RH in proportion to the Hertz-Knudsen flux (Eq 3).

pair fluctuation is detachment of a single water molecule from the surface, and the final bond-breaking is likely to be similar to (1) as captured in the Hertz-Knudsen model, and involve a net

flux balancing adsorption and desorption. This scaling was checked by scaling the value of the rate coefficient fitted at 98% RH to an estimated value at 80% RH, 3 x 10^{-35} cm^6/$molec^2$-sec. The predicted volume *vs* time curves for both RH at 293.15K are compared to data from the Kulmala simulations in Figure 3: the agreement is excellent, indicating that the temperature and RH dependences of the Hertz-Knudsen-based first order rate coefficient also apply to the third order rate coefficient.

RESULTS

The predictions of the kinetic mechanism for water evaporation are compared to experiment, predictions of the Kulmala model, and predictions of the Liu model over a temperature range of 248-318K, and RH values from 40-98%. The rate coefficients and interfacial layer thicknesses used for each set of conditions are presented in the Supplementary Material, Table S1.

The dual desorption step mechanism. The hypothesis that evaporation can be described as a combination of two simultaneous processes, first order and third order desorption, has been tested explicitly using the simulation results for the 80% RH case at 293.15K. As illustrated in Figure 4, if the evaporation mechanism is assumed to be step (1) only, the droplet radius as a function of time is predicted to be linear. This agrees with experiment at early times, but is in disagreement with the known $1/r^2$ dependence of droplet radius with time during evaporation, as well as with the Kulmala model that matches experimental data.[7, 19] The third order step (5) alone cannot describe the full time course of droplet evaporation either, although it appears to be approximately correct as the droplet becomes very small. Only simulations treating evaporation using a dual desorption step mechanism can reproduce the Kulmala and experimental data at all

points in time, establishing that these two steps constitute a minimal description of the rate-determining processes in water evaporation. This finding may partially explain why Hertz-Knudsen theory is not adequate to predict water evaporation rates: it is incomplete because it considers only first order desorption.

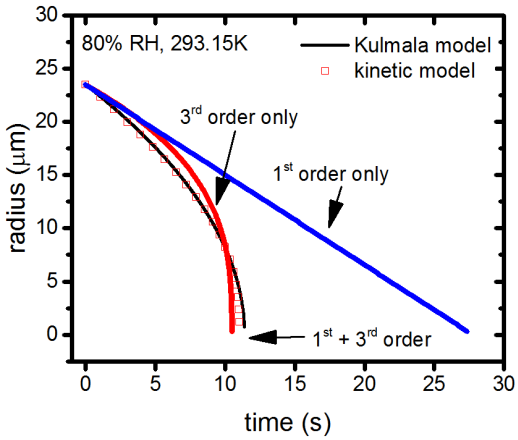

Figure 4. Plot of calculated droplet radius vs time using the Kulmala model (black solid line) and the kinetic model (red squares) for 80% RH, and a temperature of 293.15K, also presented in Figure 3. The blue line is the evaporation curve predicted if only the first order limiting case is used in the mechanism. The red line is the evaporation curve if only the third order limiting case is used.

Comparison of simulations to experiments and Kulmala predictions, varying RH and temperature. A series of calculations using the Kulmala model were made to test the kinetic model over a range of RH at a temperature of 273.15 K, and over a range of temperatures at a RH of 95% under stagnant gas (no flow) conditions. Due to a simplification in the treatment of the pure component vapour pressure and approximation of the exponential temperature dependence by a Taylor series in temperature, the Kulmala model is known to break down when

the cooling of the droplet surface below the ambient gas phase temperature exceeds 3 K.[17] The ranges in RH and temperature were chosen to ensure the degree of evaporative cooling of the droplet was always < 3 K (maximum of 0.9 K for the fixed RH simulations; maximum of 2.8 K for the fixed temperature simulations). Kinetic simulations were made for the same conditions, and the excellent agreement between those predictions and the thermodynamic Kulmala model is

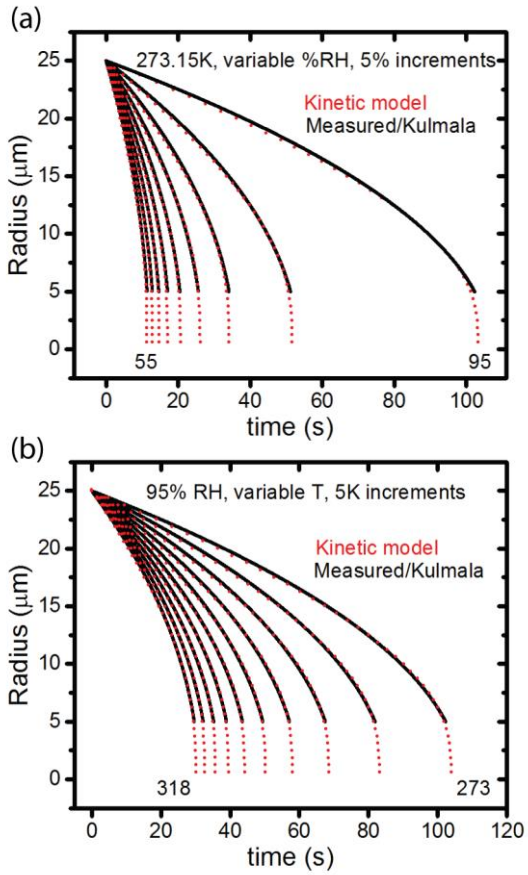

Figure 5. Comparison of predictions of the kinetic model for water evaporation to calculations using the Kulmala model, calibrated to experimental data. (a) Constant temperature, variable RH; (b) Constant RH, variable T. The rate coefficients used in the kinetic simulations are listed in Table S1.

evident in Figure 5. As described in the Methods section, the thickness of the interfacial region separating bulk water from gas phase water was treated as a fitting parameter in the simulations. The best fit values for *d* are presented in Figure 6. These values were well-fitted by an

exponential function, consistent with the trend reported in previous work.[32, 37, 42] The expression is

$$d = 10^{-10}\ (0.0001054\ e^{0.03854T}\ + 1.629) \qquad (7)$$

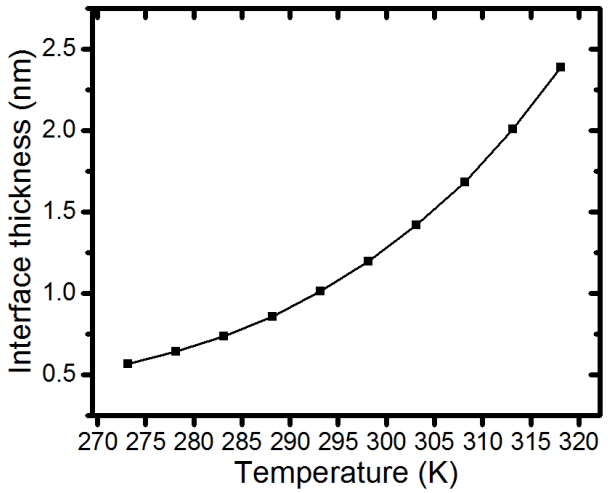

Figure 6. Estimates of interfacial thickness from the simulations in Figure 5b.

where *d* is in nm. Equation (7) was used to estimate values for *d* at temperatures outside of the fitted range in order to predict radius *vs* time curves for a set of experimental data on evaporation of supercooled water.[12] The results of the kinetic simulations are shown in Figure 7. They are in reasonable agreement over the range measured. Deviations of the predictions from the measurements are not systematic, suggesting that experimental uncertainties as well as errors due to extrapolation of the interfacial thickness outside of the fitting range may account for quantitative deviations between experiment and kinetic calculations. It should be noted that the experimental data in Figure 7 were taken under a constant gas flow over the droplet surface

which would act to enhance the evaporation rate, whereas the kinetic simulations assume a stagnant gas. For the conditions in the Figure, however, neglect of gas flow in the simulations introduces a minimal error.

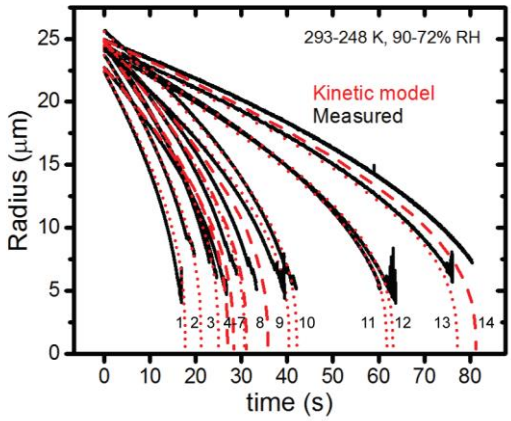

Figure 7. Predictions using the kinetic model for a range of RH and temperature combinations, compared to experimental measurements.[12] One simulation was performed for each set of experimental data obtained at a particular temperature and RH. The simulations shown with dotted lines are close to the corresponding experimental measurements, while those with dashed lines are significantly faster or slower. Left to right: 1 (283.25K, 84.2% RH), 2 (288.15K, 87.7% RH), 3 (293.15K, 90.1% RH), 4 (275K, 82.9% RH), 5 (278.85K, 88.1% RH), 6 (273.85K, 83.7% RH), 7 (270.95K, 82.1% RH), 8 (272.85K, 85.3% RH), 9 (262.45K, 78.9% RH), 10 (265.3K, 81% RH), 11 (258.15K, 82.3% RH), 12 (267.45K, 89.6% RH), 13 (254.2K, 81.3% RH), 14 (248.25K, 72% RH).

Evaporation at reduced RH. As noted above, the accuracy of the Kulmala model[7] deteriorates under conditions where surface cooling due to the energetics of evaporation is <3 K.[17, 18, 21, 47] Measurements of droplet cooling[13] have been made for water droplets evaporating into dry nitrogen, and nitrogen humidified to >80% RH. The data show that cooling in the range of 17 K takes place when the surrounding gas is dry, and that cooling during evaporation into humid nitrogen is minimal. Data for the intermediate range are not available, but simulations using

alternative models such as the Liu model that take into account heat as well as mass flux, provide estimates as a function of temperature and RH.[18, 47] As shown in Figures 5 and 7, the 3 step kinetic mechanism is consistent with the Kulmala model for a wide range of temperature and RH conditions over which the model can be used. The Liu model more accurately reflects the heat fluxes incurred at the higher evaporation rates associated with reduced RH and/or higher temperatures. A thorough comparison between the Liu model and the kinetic description was made over a broad temperature range spanning 278 – 293 K, and RH from 40 – 75% in order to investigate the agreement between the two models under conditions where the surface cooling was > 3K. Representative results are shown in Figure 8 for 278 and 293K.

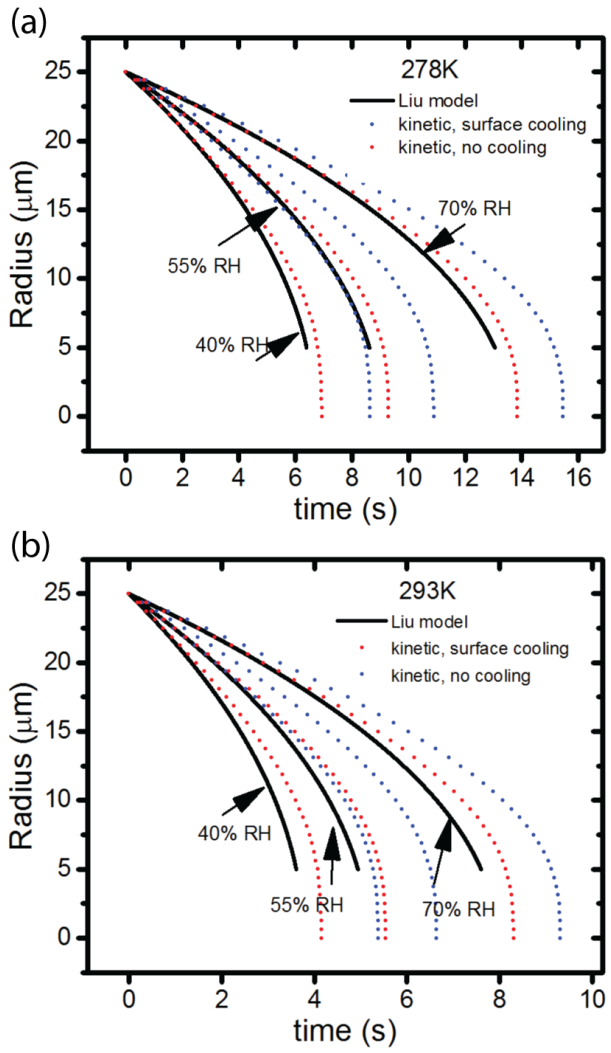

Figure 8. Comparison of predicted evaporation curves using the Liu model, which takes evaporative surface cooling into account, and kinetic model calculations with (blue symbols) and without (red symbols) evaporative surface cooling. (a) Surface temperature of 278K (no cooling), and 275.7K (70% RH), 274.5K (55% RH), and 273.2K (40% RH). (b) Surface temperature of 293K (no cooling), and 289.2K (70% RH), 287.1K (55% RH), and 284.8K (40% RH).

The kinetic simulations (red symbols) for this range of conditions are not in as good agreement with the Liu model as they were with the Kulmala model over the relevant conditions of temperature and RH, where evaporation is relatively slow. The Liu model predicts a faster

evaporation rate than the kinetic model, with increasing differences as gas phase temperature is increased.

To test whether the discrepancy between the kinetic model and the Liu model is due to neglect of explicit treatment of heat flux in the kinetic description, additional simulations were made assuming the estimated surface temperature from the Liu model, shown in Figure 8. In all cases, inclusion of rate coefficients calculated for lower temperatures slows evaporation, and increases the disagreement between the Liu and kinetic models.

DISCUSSION

The kinetic description brings together fundamental elements in the literature into a single model that is predictive across time and length scales for a broad range of conditions. The very simple representation developed in this work incorporates detailed molecular-level physics including the existence of a diffuse interface separating vapor from liquid, which are embodied in the stoichiometries of the steps and their rate coefficients. Accordingly, a more unified picture of water evaporation emerges. The liquid-vapor interface of water is diffuse, extending from a region that has the bulk structure of water through a zone with disrupted hydrogen bonds, to a zone with free water molecules, to the gas phase. This zone is not static, but has continual fluctuations detected as capillary waves that make the water desorption process more complex than simply rupture of hydrogen bonds. The continuum of local interactions identified by theory can be approximated as the sum of two limiting desorption cases in order to match macroscopic experimental observations. Both cases should be seen as involving a passage through the interfacial region as well as hydrogen bond-breaking, not simply a local event at a well-defined

boundary as would be expected for solid state interfaces. While this region is not abrupt, its characteristic dimension is less than the mean free path of gases at atmospheric pressure, about 70 nm. This means the passage does not involve molecular collisions, only the influences of the potential energy surface as the water fluctuates and decreases in density.

The relative importance of the 1st and 3rd order steps as a function of time and droplet size can be assessed using the kinetic simulations. The stochastic algorithm permits insertion of markers into the reaction steps to track how often they occur and dissect how competing pathways interact, facilitating a deeper analysis of the simulation results.[56-58] In the present simulations, the surface region of the liquid is held constant in thickness, and therefore volume, as evaporation proceeds. As the droplet shrinks in size, its surface to volume ratio increases and therefore the total concentration of waters in the surface region increases: higher order kinetics such as the third order step have a higher rate than that of the first order step, and become dominant. The surface to volume ratio and the contributions of the two steps to formation of vapor phase water are shown as a function of time in Figure 9 for a typical set of conditions.

The data show that although the shapes of the evaporation curves shown in Figure 4 seem to indicate that at early and late times only one of the reaction steps might be needed to fully represent evaporation, in fact both are active at all times and together control the evaporation process. Interestingly, the assumption that both the 1st and 3rd order steps scale in the same way with RH and temperature holds across a broad range of conditions. This supports the physical picture that the model's two steps represent limiting cases of a continuum of interactions that

precede water desorption, and that inclusion of two these cases only is sufficient to describe macroscopic observations.

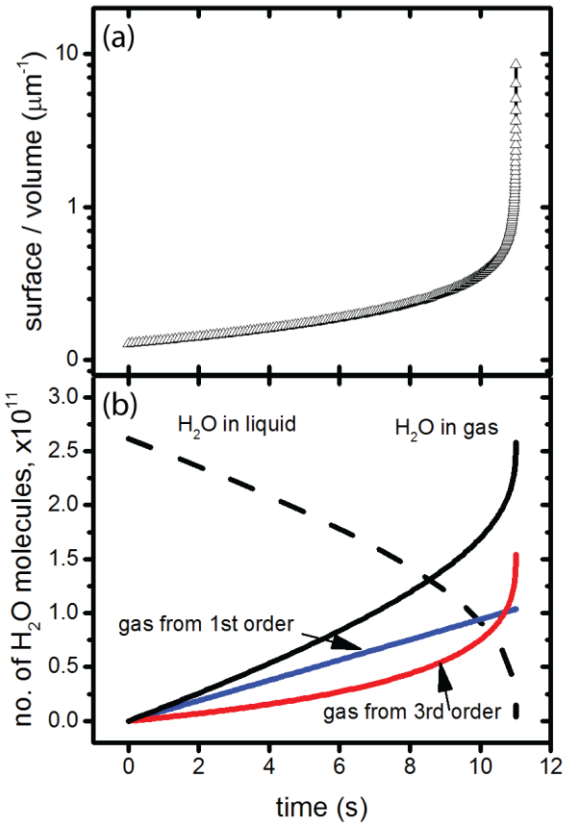

Figure 9. Evolution of droplet at 293.15K, 80% RH. (a) Surface to volume ratio. (b) Breakdown of 1st and 3rd order water desorption process contributions to evaporation as the droplet size decreases.

The question of the role of heat flux and surface cooling during evaporation is not settled in this work. The kinetic model assumes that the entire droplet is isothermal, and at the same temperature as the surrounding vapor at all times. Heat flow, which would be reflected in temperature dependent rate constants and direct tracking of energy consumed due to net evaporation, is neglected. The kinetic simulations are compared throughout to thermodynamic models, the Kulmala and Liu models, that explicitly include coupled heat and mass flows during

evaporation. All the models, thermodynamic and kinetic, have in common a dependence on water concentration gradients and vapor pressures and lead to a macroscopic description consistent with experiment. The agreement is quantitative with the Kulmala model, and the simulations are predictive for measurements under diverse combinations of RH and temperature where the degree of surface cooling is less than 3K. This agreement suggests that, at least in this range, the combination of the 1st and 3rd order steps and inclusion of an interfacial zone of finite thickness may constitute an equivalent description to the water vapor-controlled physics captured in the thermodynamics-based models, and that energy flows are not kinetically significant. How well the kinetic model can describe evaporation into partially dry and/or warm gas, where droplet surface cooling is more pronounced and evaporation is more rapid, has not been fully determined in this work. Considering together the results from all three sets of simulations, where the kinetic model provides a self-consistent means of intercomparison over the entire range of conditions, it is clear that there are differences in the predictions that cannot be attributed solely to whether or not surface cooling is taken into account. These differences must originate in other aspects of the model constructions, potentially from additional missing physics as RH is varied. The experimental technique for measuring the evaporation of water and water-based solutions references droplets of different composition to each other to determine the actual RH for the measurement in the mid-RH range.[18] Direct independent measurements of ambient water concentration are only available for high RH (where cooling is minimal) and near-zero RH (where it can be substantial for droplets, but not for large water pools).[13, 27] Detailed measurements using gas streams of precisely known RH that has been measured independently, for example by cavity ring-down spectroscopy, would be invaluable to identify the physical origin of the differences in model predictions, and to understand the role of surface cooling in

controlling evaporation when its rate is fast. It should be noted that evaporation into a vacuum, where condensation does not occur and surface cooling is significant,[27] would not be properly described using this kinetic scheme. Adaptations of the model for this case can be developed if experimental data are available for validation.

The simple, single compartment model used here can in principle be extended to a multicompartment model with subnanometer resolution, allowing exploration of how evaporation kinetics, surface tension and the Kelvin effect are intertwined as the droplet's volume decreases to zero. In practice, the rapid diffusion of water throughout the volume, which continuously exchanges water locations and is treated as instantaneous in a single compartment model, would be prohibitively expensive using a stochastic algorithm. A practical limit has been found to be liquids where the self-diffusion coefficient is about 100x slower than water using modeling techniques available today.[59] This class of algorithms has the advantage of being able to simulate continuously shrinking volumes over long times, but is very inefficient when rapid mixing and slow processes such as reactions and desorption are coupled. Innovations in mechanism design are required to enable fully spatially resolved simulations to be performed.

CONCLUSIONS

A simple 3-step kinetic scheme has been developed that describes the evaporation kinetics of pure water as being a process of movement of water into the near-surface region of a droplet, and desorption from the surface into the gas phase via two parallel and competing pathways. The scheme has been compared to experiment and several evaporation models (Hertz-Knudsen, Kulmala and Liu) over a broad range of temperatures and relative humidity. Direct comparison

of radius vs time curves shows excellent agreement with the experimental data and Kulmala simulations, poor agreement with the Hertz-Knudsen model except at early times, and systematic disagreement with the Liu model, which always predicts a higher flux than the kinetic model. The physical origin of disagreement between the kinetic and Liu models remains to be determined. This simple kinetic scheme is well-grounded in molecular theory, and serves to connect it to macroscopic observations in a predictive way. Combination of it with chemical reactions and other phenomena such as water transport through condensed phases will allow the influence of local concentrations on reactivity to be assessed more accurately.

SUPPLEMENTARY MATERIAL

See Supplementary Material for complete information on parameters used in the simulations.

ACKNOWLEDGMENTS

This material is based upon work performed by the Joint Center for Artificial Photosynthesis, a DOE Energy Innovation Hub, supported through the Office of Science of the U.S. Department of Energy under Award Number DE-SC0004993, where efforts focused on establishment of a quantitative model (FAH and CJP). This work was initiated under the Laboratory Directed Research and Development Program of the Department of Energy's Lawrence Berkeley National Laboratory under U. S. Department of Energy Office of Science, Office of Basic Energy Sciences, under Contract No. DE-AC02-05CH11231. C.J.P. sincerely thanks the Cal Energy Corps for a summer internship (2018). JPR and REHM acknowledge financial support from the EPSRC (UK) through grant EP/N025245/1.

AUTHOR CONTRIBUTIONS

FAH and JPR conceived of this study. REHM and JPR provided experimental and computational data, and FAH developed the initial kinetic model for comparison to them and refinements were made with CJP. All authors participated in analysis of the results and contributed to the submitted version of the paper.

DATA AVAILABILITY STATEMENT

All data used for preparation of the figures in this work are included in a Supplementary Material file.

REFERENCES

1. F. R. Newbold and N. R. Amundson, Aiche Journal **19** (1), 22-30 (1973).
2. J. Julin, M. Shiraiwa, R. E. H. Miles, J. P. Reid, U. Poschl and I. Riipinen, Journal of Physical Chemistry A **117** (2), 410-420 (2013).
3. G. Fang and C. A. Ward, Physical Review E **59** (1), 441-453 (1999).
4. G. Fang and C. A. Ward, Physical Review E **59** (1), 417-428 (1999).
5. P. Varilly and D. Chandler, Journal of Physical Chemistry B **117** (5), 1419-1428 (2013).
6. A. H. Persad and C. A. Ward, Chemical Reviews **116** (14), 7727-7767 (2016).
7. M. Kulmala, T. Vesala and P. E. Wagner, Proceedings of the Royal Society of London Series a-Mathematical Physical and Engineering Sciences **441** (1913), 589-605 (1993).
8. T. Vesala, M. Kulmala, R. Rudolf, A. Vrtala and P. E. Wagner, Journal of Aerosol Science **28** (4), 565-598 (1997).

9. A. Braslau, P. S. Pershan, G. Swislow, B. M. Ocko and J. Alsnielsen, Physical Review A **38** (5), 2457-2470 (1988).

10. P. Innocenzi, L. Malfatti, M. Piccinini, A. Marcelli and D. Groso, Journal of Physical Chemistry A **113** (12), 2745-2749 (2009).

11. K. R. Wilson, M. Cavalleri, B. S. Rude, R. D. Schaller, A. Nilsson, L. G. M. Pettersson, N. Goldman, T. Catalano, J. D. Bozek and R. J. Saykally, Journal of Physics-Condensed Matter **14** (8), L221-L226 (2002).

12. J. F. Davies, R. E. H. Miles, A. E. Haddrell and J. P. Reid, Journal of Geophysical Research-Atmospheres **119** (18), 10931-10940 (2014).

13. C. Heinisch, J. B. Wills, J. P. Reid, T. Tschudi and C. Tropea, Physical Chemistry Chemical Physics **11** (42), 9720-9728 (2009).

14. R. Holyst, M. Litniewski and D. Jakubczyk, Soft Matter **13** (35), 5858-5864 (2017).

15. R. Holyst, M. Litniewski, D. Jakubczyk, M. Zientara and M. Wozniak, Soft Matter **9** (32), 7766-7774 (2013).

16. Y. Q. Li, P. Davidovits, Q. Shi, J. T. Jayne, C. E. Kolb and D. R. Worsnop, Journal of Physical Chemistry A **105** (47), 10627-10634 (2001).

17. G. Rovelli, R. E. H. Miles, J. P. Reid and S. L. Clegg, Journal of Physical Chemistry A **120** (25), 4376-4388 (2016).

18. Y. Y. Su, R. E. H. Miles, Z. M. Li, J. P. Reid and J. Xu, Physical Chemistry Chemical Physics **20** (36), 23453-23466 (2018).

19. D. J. Woodland and E. Mack, Journal of the American Chemical Society **55**, 3149-3161 (1933).

20. M. Zientara, D. Jakubczyk, K. Kolwas and M. Kolwas, Journal of Physical Chemistry A **112** (23), 5152-5158 (2008).

21. R. E. H. Miles, J. P. Reid and I. Riipinen, Journal of Physical Chemistry A **116** (44), 10810-10825 (2012).

22. L. C. Weng, A. T. Bell and A. Z. Weber, Energy & Environmental Science **12** (6), 1950-1968 (2019).

23. P. Davidovits, D. R. Worsnop, J. T. Jayne, C. E. Kolb, P. Winkler, A. Vrtala, P. E. Wagner, M. Kulmala, K. E. J. Lehtinen, T. Vesala and M. Mozurkewich, Geophysical Research Letters **31** (22) (2004).

24. I. W. Eames, N. J. Marr and H. Sabir, International Journal of Heat and Mass Transfer **40** (12), 2963-2973 (1997).

25. R. Marek and J. Straub, International Journal of Heat and Mass Transfer **44** (1), 39-53 (2001).

26. R. Meland, A. Frezzotti, T. Ytrehus and B. Hafskjold, Physics of Fluids **16** (2), 223-243 (2004).

27. J. D. Smith, C. D. Cappa, W. S. Drisdell, R. C. Cohen and R. J. Saykally, Journal of the American Chemical Society **128** (39), 12892-12898 (2006).

28. C. A. Ward and G. Fang, Physical Review E **59** (1), 429-440 (1999).

29. K. H. Ahn and B. Y. H. Liu, Journal of Aerosol Science **21** (2), 249-261 (1990).

30. P. Jafari, A. Amritkar and H. Ghasemi, Journal of Physical Chemistry C **124** (2), 1554-1559 (2020).

31. M. A. Kazemi, D. S. Nobes and J. A. W. Elliott, Langmuir **33** (18), 4578-4591 (2017).

32. F. Caupin, Physical Review E **71** (5), 051605 (2005).

33. L. X. Dang and T. M. Chang, Journal of Chemical Physics **106** (19), 8149-8159 (1997).

34. M. R. Feeney and P. G. Debenedetti, Industrial & Engineering Chemistry Research **42** (25), 6396-6405 (2003).

35. B. C. Garrett, G. K. Schenter and A. Morita, Chemical Reviews **106** (4), 1355-1374 (2006).

36. M. J. P. Nijmeijer, C. Bruin, A. B. Vanwoerkom, A. F. Bakker and J. M. J. Vanleeuwen, Journal of Chemical Physics **96** (1), 565-576 (1992).

37. M. Sega and C. Dellago, Journal of Physical Chemistry B **121** (15), 3798-3803 (2017).

38. S. M. Thompson, K. E. Gubbins, J. P. R. B. Walton, R. A. R. Chantry and J. S. Rowlinson, Journal of Chemical Physics **81** (1), 530-542 (1984).

39. R. C. Tolman, Journal of Chemical Physics **17** (3), 333-337 (1949).

40. R. C. Tolman, Journal of Chemical Physics **17** (2), 118-127 (1949).

41. L. B. Partay, G. Hantal, P. Jedlovszky, A. Vincze and G. Horvai, Journal of Computational Chemistry **29** (6), 945-956 (2008).

42. K. Kinosita and H. Yokota, Journal of the Physical Society of Japan **20** (6), 1086 (1965).

43. O. Wohlfahrt, C. Dellago and M. Sega, Journal of Chemical Physics **153** (14) (2020).

44. M. J. Liu, A. A. Wiegel, K. R. Wilson and F. A. Houle, Journal of Physical Chemistry A **121** (31), 5856-5870 (2017).

45. R. D. Davis, M. I. Jacobs, F. A. Houle and K. R. Wilson, Analytical Chemistry **89** (22), 12494-12501 (2017).

46. Y. Nagata, K. Usui and M. Bonn, Physical Review Letters **115** (23) (2015).

47. Y. Y. Su, A. Marsh, A. E. Haddrell, Z. M. Li and J. P. Reid, Journal of Geophysical Research-Atmospheres **122** (22), 12317-12334 (2017).

48. W. D. Hinsberg and F. A. Houle, (www.hinsberg.net/kinetiscope, 2018).

49. D. L. Bunker, B. Garrett, T. Kleindienst and G. S. Long, Combust Flame **23** (3), 373-379 (1974).

50. D. T. Gillespie, J Atmos Sci **32** (10), 1977-1989 (1975).

51. W. Wagner and A. Pruss, Journal of Physical and Chemical Reference Data **22** (3), 783-787 (1993).

52. P. M. Winkler, A. Vrtala, P. E. Wagner, M. Kulmala, K. E. J. Lehtinen and T. Vesala, Physical Review Letters **93** (7) (2004).

53. D. M. Murphy and T. Koop, Quarterly Journal of the Royal Meteorological Society **131** (608), 1539-1565 (2005).

54. J. L. Shereshefsky and S. Steckler, Journal of Chemical Physics **4** (2), 108-115 (1936).

55. K. Tanaka, Journal of the Chemical Society-Faraday Transactions I **71** (5), 1127-1131 (1975).

56. T. P. Cheshire, M. K. Brennaman, P. G. Giokas, D. F. Zigler, A. M. Moran, J. M. Papanikolas, G. J. Meyer, T. J. Meyer and F. A. Houle, Journal of Physical Chemistry B **124** (28), 5971-5985 (2020).

57. F. A. Houle, Journal of Physical Chemistry C **123** (23), 14459-14467 (2019).

58. F. A. Houle, A. A. Wiegel and K. R. Wilson, Journal of Physical Chemistry Letters **9** (5), 1053-1057 (2018).

59. F. A. Houle, W. D. Hinsberg and K. R. Wilson, Physical Chemistry Chemical Physics **17** (6), 4412-4423 (2015).